# Squaring cooperative binding circles

Alexander B. C. Deutman[a], Cyrille Monnereau[a], Mohamed Moalin[a], Ruud G. E. Coumans[a], Nico Veling[a], Michiel Coenen[a], Jan M. M. Smits[a], René de Gelder[a], Johannes A. A. W. Elemans[a], Gianfranco Ercolani[b], Roeland J. M. Nolte[a,1], and Alan E. Rowan[a,1]

[a]Institute for Molecules and Materials, Radboud University Nijmegen, Toernooiveld 1, 6525ED Nijmegen, The Netherlands; and [b]Dipartimento di Scienze e Tecnologie Chimiche, Università di Roma Tor Vergata, Via della Ricerca Scientifica, 00133 Rome, Italy

Edited by Julius Rebek, Jr., The Scripps Research Institute, La Jolla, CA, and approved March 14, 2009 (received for review October 10, 2008)

**The cooperative binding effects of viologens and pyridines to a synthetic bivalent porphyrin receptor are used as a model system to study how the magnitudes of these effects relate to the experimentally obtained values. The full thermodynamic and kinetic circles concerning both activation and inhibition of the cage of the receptor for the binding of viologens were measured and evaluated. The results strongly emphasize the apparent character of measured binding and rate constants, in which the fractional saturation of receptors with other guests is linearly expressed in these constants. The presented method can be used as a simple tool to better analyze and comprehend the experimentally observed kinetics and thermodynamics of natural and artificial cooperative systems.**

kinetics | slippage | supramolecular chemistry | thermodynamics

Cooperative binding plays an important role in nature, where it is used to construct well-defined assemblies and is used as a tool to transfer information at the cellular level (1). The formation of the tobacco mosaic virus (2) and the binding of oxygen to hemoglobin (3) are 2 well-known examples of cooperative processes. Cooperative binding interactions can be homotropic or heterotropic, when the combined binding to a multivalent receptor involves the same or different types of guests. In additions, these interactions can be positive or negative, when the binding of a guest promotes or obstructs the binding of a second guest (4).

One of the challenges in the field of supramolecular chemistry is to design artificial systems that display cooperative binding effects, not only to better understand the mechanisms involved in the natural processes but also to prepare functional materials and catalysts that benefit from such binding interactions. Over the years, a large number of artificial receptors displaying positive (5–8) and negative (9–11) homotropic and positive (12–20) and negative (21–23) heterotropic cooperative binding phenomena have been developed. Although in many cases the origins of the cooperative effects could be identified, few studies have dealt in detail with the kinetics and thermodynamics of such complicated multicomponent receptor–guest systems. This is surprising, because unlike the complex biological systems, the artificial receptor–guest systems can be easily studied, and the fine details of cooperative behavior can be uncovered. It is generally known that measured association constants are context dependent in the sense that apparent values that depend on, e.g., the solvent system, salt concentrations, pH, and in the worst case impurities, are obtained (4). As a consequence, the observed cooperative binding effects might often deviate from the intrinsic ones.

To investigate how the measured cooperative binding effects as derived from the observed experimental binding constants are related to the intrinsic ones, we present a detailed study of the combined binding of viologens and pyridines to the bivalent zinc porphyrin receptor **Zn1** (24, 25) (Scheme 1). Pyridine ligands can activate and inhibit the binding of viologens in the cavity of **Zn1** (see Fig. 1). These compounds also affect the kinetics of pseudorotaxane formation [slippage (26–29) experiments] between **Zn1** and a stopper functionalized viologen derivative. The present study aims at providing a simple and efficient procedure for deriving cooperative binding effects from experimentally obtained kinetic and thermodynamic data to be used as a guide in other artificial and natural cooperative binding systems. The procedure relies on the apparent 1:1 binding character of experimentally obtained binding constants that can be expected under the chosen experimental conditions. With the use of this method, complete multicomponent binding circles can be accurately and simply derived from a series of simple apparent 1:1 binding experiments.

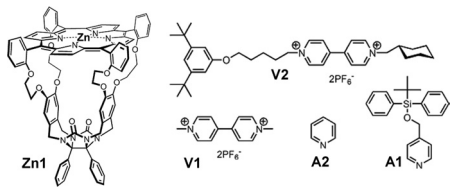


**Scheme 1.** Host and guest compounds.

## Results and Discussion

Porphyrin macrocycle **Zn1** (24) binds viologen derivatives in its cavity with high binding constants ($K_{assoc}$ = $10^6$ to $10^7$ $M^{-1}$) in organic solvents and can also complex pyridine derivatives to the zinc metal in the porphyrin roof. A bulky pyridine (e.g., **A1**) coordinates weakly to the outside of **Zn1**. Pyridine (**A2**) on the other hand, binds strongly to the inside of the cavity of **Zn1** as a result of size complementarity, $\pi$–$\pi$ stacking interactions, and metal–ligand coordination (see crystal structure in Fig. 1*E*). In a previous article (17), it was shown that the bulky *tert*-butylpyridine and methylviologen (**V1**) display strong positive cooperative effects in their binding to **Zn1**. The complexation behavior of pyridines and viologens to **Zn1** can be studied easily with $^1$H NMR, fluorescence, and UV-vis spectroscopy. This model system therefore is ideal to unravel the full cooperative binding circles. We can either activate (with a bulky pyridine) or inhibit (with pyridine) the cavity of **Zn1** to bind viologen derivatives (Fig. 1 *A* and *B*). In addition, we can study both directions of the binding circles, i.e., the effect of the binding of pyridines on the receptor–viologen binding strength and the effect of the binding of viologen derivatives on the receptor–pyridine binding strength. Although Hess's law predicts that a cooperative effect should be equal and independent of the measured direction of such a circle, this will not be the case for the experimentally determined (apparent) cooperative effects as will be illustrated in the following.

Author contributions: A.B.C.D., J.A.A.W.E., R.J.M.N., and A.E.R. designed research; A.B.C.D., C.M., M.M., N.V., J.M.M.S., R.d.G., and J.A.A.W.E. performed research; A.B.C.D., R.G.E.C., M.C., J.M.M.S., R.d.G., and G.E. analyzed data; and A.B.C.D., G.E., R.J.M.N., and A.E.R. wrote the paper.

The authors declare no conflict of interest.

This article is a PNAS Direct Submission.

Data deposition: The atomic coordinates have been deposited in the Cambridge Crystallographic Data Centre, www.ccdc.cam.ac.uk (CCDC ID code: CCDC 725495.)

[1]To whom correspondence may be addressed. E-mail: r.nolte@science.ru.nl or a.rowan@science.ru.nl.

This article contains supporting information online at www.pnas.org/cgi/content/full/0810145106/DCSupplemental.

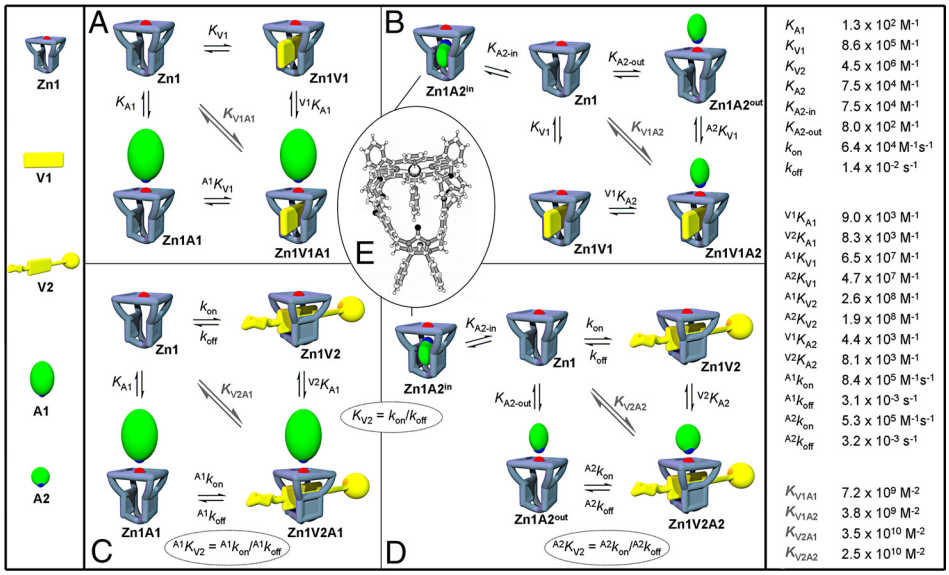


**Fig. 1.** Cartoon representation of the binding schemes showing the cooperative binding effects together with the individual rate and association constants. (*A*) Cooperative binding circle involving **V1**, **A1**, and **Zn1**. (*B*) Competitive cooperative binding circle involving **V1**, **A2**, and **Zn1**. (*C*) Cooperative binding circle involving **A1** and slippage of **Zn1** over the cyclohexyl moiety of **V2**. (*D*) As in *C* involving **A2**, **V2**, and **Zn1**. (*E*) Crystal structure of the complex between **Zn1** and pyridine. All of the calculated constants presented are listed on the right (for experimental errors see Table S1).

To be able to monitor the cooperative effects also on the kinetics of complex formation, we performed studies with the dumbbell-shaped viologen derivative **V2**. **V2** has a di-*tert*-butylphenyl moiety attached to one side that cannot be traversed by **Zn1** and a cyclohexyl moiety attached to the other side, which can be passed over via a slippage (26–29) process. The kinetics of this complex formation can be monitored accurately with the help of fluorescence spectroscopy.

Ideally, one would like to determine the magnitudes of cooperative effects from a single experiment in which the changing ratios of the different receptor/guest species can be monitored, and fitting to the full binding model would provide the association constant of the ternary complex, the individual equilibrium constants, and the cooperative effect. Such a method requires that all of the relevant species of receptor (free, the 2 1:1 complexes, and the ternary complex) can be identified and quantified spectroscopically, after which, curve-fitting should be fairly straightforward but not necessarily very accurate as a result of the determination of multiple constants from a single fit. Unfortunately, binding systems displaying such spectroscopic properties are very rare. Certainly our system does not allow the precise identification of all of the changing ratios from a single experiment as a result of the high association constant of **Zn1** with viologens (that allows for accurate determination only at micromolar concentrations), the fast exchanging zinc–pyridine interaction on the NMR time scale, and the overlapping fluorescence and UV-vis spectra of the different porphyrin species.

For this reason, we chose a strategy in which the consecutive binding steps necessary to form the ternary complex were individually evaluated. This requires binding experiments of the 1:1 complexes between the receptor and the individual guests ($K_{G1}$ and $K_{G2}$) and a binding experiment in which the affinity of a guest to the receptor is studied in the presence of an excess of the other guest ($^{G1}K_{G2}$ or $^{G2}K_{G1}$). By determining the 3 association constants $K_{G1}$, $K_{G2}$, and $^{G1}K_{G2}$ (all in $M^{-1}$), the association constant of the ternary complex (in $M^{-2}$) and the cooperative effect (*Ce*) can be identified ($K_{G1G2} = K_{G1}\cdot{}^{G1}K_{G2} = K_{G2}\cdot{}^{G2}K_{G1}$). Analysis of the different binding systems (Fig. 1) with the use of this method is presented in the following.

**Thermodynamic Cooperative Circles.** The cooperative binding circle involving **Zn1**, **V1**, and **A1** is presented in Fig. 1*A*. $^1$H NMR and UV-vis titrations in 1:1 (vol/vol) mixtures of chloroform and acetonitrile (deuterated solvents in the case of the NMR experiments) revealed that **A1** binds weakly ($K_{A1}$ = 125 $M^{-1}$) and exclusively to the outside of the cage of **Zn1**. A $^1$H NMR titration revealed an association constant $^{V1}K_{A1}$ of 9.0 × $10^3$ $M^{-1}$ for the binding of **A1** to **Zn1** in the presence of a slight excess of **V1**, which fully occupies the cavity of **Zn1**. The cooperative effect ($Ce = {}^{V}K_A/K_A$) therefore has a value of 72 ($\Delta\Delta G^o = -10.6$ kJ/mole). The reverse direction of the circle (i.e., the effect of the presence of **A1** on the binding of **V1** in **Zn1**) was also measured. In order be able to accurately determine the high association constant between **Zn1** and **V1**, the titration experiments were performed at low (less than micromolar) concentrations of **Zn1** and monitored by fluorescence spectroscopy. The viologen-induced quenching of the porphyrin emission upon complex formation was monitored in the presence of various concentrations of **A1**. All titration curves could be fitted with the help of simple 1:1 binding isotherms. The titration experiments clearly revealed that the observed association constant of the complex between **V1** and **Zn1** ($^{A1}K_{V1\text{-app}}$) increases upon increasing concentrations of **A1** (see Fig. 2) in line with the apparent character of $^{A1}K_{V1\text{-app}}$. It can be easily derived that the apparent association

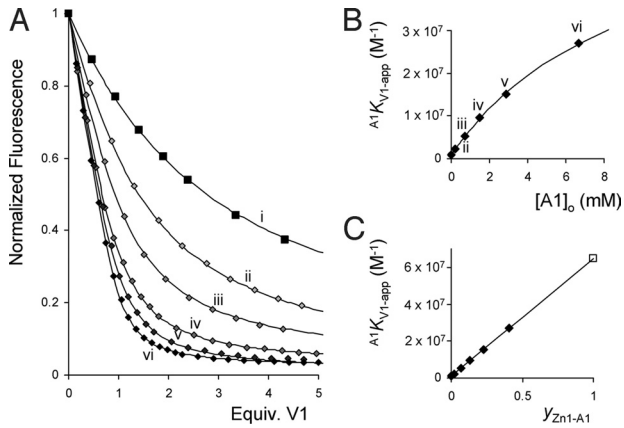


**Fig. 2.** Fluorescence titrations of **V1** with **Zn1** in the presence of various concentrations of **A1**. (*A*) Titration of **V1** to **Zn1** in the presence of increasing concentrations (from *i* to *vi*) of **A1** and the fits according to 1:1 binding isotherms. (*B*) Calculated association constant $^{A1}K_{V1\text{-app}}$ plotted vs. the concentration of **A1** and the fit of the data points using Eq. **1**. (*C*) Linear relationship between of the value of $^{A1}K_{V1\text{-app}}$ and the fractional saturation of **Zn1** with **A1** ($y_{Zn1\text{-}A1}$) according to Eq. **3**.

constant in the presence of different concentrations of **A1** ($^{A1}K_{V1\text{-}app}$) should evolve according to Eq. **1**.

$$^{A1}K_{V1-app} = \frac{K_{V1}+[A1]\cdot K_{A1}\cdot{}^{A1}K_{V1}}{1+[A1]\cdot K_{A1}}. \quad [1]$$

Because the total concentration of **A1** ($[A1]_o$) is much larger than the concentration of **Zn1**, hence $[A1] \approx [A1]_o$ (which also accounts for the apparent 1:1 binding behavior), and therefore Eq. **1** can be used to determine the actual value of $^{A1}K_{V1}$. A fit of the experimental data provided values of $^{A1}K_{V1} = 6.5 \times 10^7\ M^{-1}$ (hence a value of $Ce = 75$ because $K_{V1} = 8.6 \times 10^5\ M^{-1}$) and $K_{A1} = 103\ M^{-1}$ (See Fig. 2*B*). These data are within experimental error in accordance with the values obtained for the other direction of the circle of $Ce = 72$ and $K_{A1} = 125\ M^{-1}$. As a result, also the association constants of the ternary complex $K_{V1A1}$ (Fig. 1*A*) are equal within experimental error (clockwise: $K_{V1A1} = 7.7 \times 10^9\ M^{-2}$, counterclockwise $K_{V1A1} = 6.7 \times 10^9\ M^{-2}$, a difference of <0.4 kJ/Mole in Gibbs free binding energy). This thus demonstrates that, although the experimentally determined cooperative effects measured by fluorescence never revealed the full cooperative effect, the overall system behaves according to Hess's law and that the binding circle is perfectly balanced as required by thermodynamics. The experimentally obtained apparent association constant when titrating **V1** into a mixture of **Zn1** and an excess of **A1** depends linearly (see Eq. **3**) on the fractional saturation (30) of the receptor with the second guest ($y_{Zn1\text{-}A1}$). The fractional saturation is defined as the fraction of the total number of receptor molecules R that are occupied by a particular guest G (Eq. **2**). This linear relation ship is clearly expressed in Fig. 2*C*.

$$y_{R-G} = \frac{K_G[G]}{1+K_G[G]} = \frac{[RG]}{[R]+[RG]} \quad [2]$$

$$^{A1}K_{V1-app} = K_{V1}\cdot\{1+y_{Znl\text{-}A1}\cdot(Ce-1)\}. \quad [3]$$

Because pyridine (**A2**) coordinates strongly to the inside of the cage of **Zn1** ($K_{A2} = 7.5 \times 10^4\ M^{-1}$), it can be expected to compete with **V1** for this binding position. On the other hand, **A2** should also be capable of binding to the outside of **Zn1** and hence can have a positive cooperative effect on the binding of **V1** in a similar way to **A1** (see Fig. 1*B*). Fluorescence titrations in which **V1** was added to **Zn1** were performed in the presence of increasing concentrations of **A2**. Also in this case, the binding isotherms could all be fitted to 1:1 binding models. The data clearly revealed that the apparent association constant ($^{A2}K_{V1\text{-}app}$) decreases in the presence of increasing concentrations of **A2** (See Fig. 3). Assuming the binding scheme of Fig. 1*B*, the apparent association constant $^{A2}K_{V1}$ should evolve according to Eq. **4**, in which $K_{A2\text{-}out}$ is the association constant of the complex of **A2** to the outside of **Zn1** and $K_{A2\text{-}total}$ the sum of the association constants of the complexes in which **A2** binds to the inside and outside of **Zn1** ($K_{A2\text{-}total} = K_{A2\text{-}in} + K_{A2\text{-}out}$).

$$^{A2}K_{V1-app} = \frac{K_{V1}+[A2]\cdot K_{A2-out}\cdot{}^{A2}K_{V1}}{1+[A2]\cdot K_{A2-Total}}. \quad [4]$$

With the help of Eq. **5**, the magnitude of $K_{A2\text{-}out}\cdot{}^{A2}K_{V1}$ (equal to $K_{V1A2} = 3.8 \times 10^9\ M^{-2}$), and $K_{A2\text{-}total}$ (equal to $7.1 \times 10^4\ M^{-1}$) could be calculated. Also here, the value of $K_{A2\text{-}total}$ is in good agreement with the directly measured value of this association constant ($K_{A2\text{-}total} = 7.5 \times 10^4\ M^{-1}$). Assuming that **A2** has an association constant for the outside of the cavity of **Zn1** that is slightly lower than that of **A1** ($80 \pm 15\ M^{-1}$),* the data suggest a strong positive cooperative effect ($Ce = 54$) for the combined

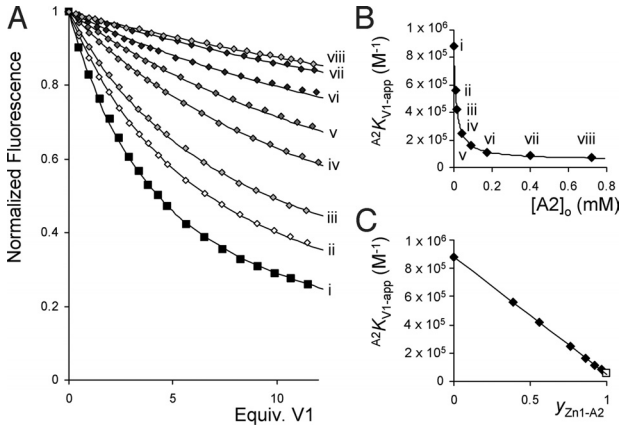


**Fig. 3.** Fluorescence titrations of **V1** with **Zn1** in the presence of **A2**. (*A*) Titration curves of **V1** to **Zn1** in the presence of increasing concentrations (from *i* to *viii*) of **A2** and the fits according to 1:1 binding isotherms. (*B*) Calculated association constant $^{A2}K_{V1\text{-}app}$ plotted vs. the concentration of **A2** and the fit of the data points using Eq. **4**. (*C*) Linear relationship between the value of $^{A2}K_{V1\text{-}app}$ and the fractional saturation of **Zn1** with **A2** ($y_{Zn1\text{-}A2}$) according to Eq. **5**.

binding of **V1** and **A2** to **Zn1**. Although pyridine blocks the cavity of **Zn1** when it is bound in it, it causes a similar positive cooperative effect as **A1** for the binding of **V1** to **Zn1** when it is coordinated to the outside. Also in this competition experiment, the obtained apparent association constant depends linearly on the fractional saturation of **Zn1** with **A2** ($y_{Zn1\text{-}A2}$), according to Eq. **5**, as can be seen in Fig. 3*C*.

$$^{A2}K_{V1-app} = K_{V1} + y_{Znl-A2}\cdot\left(\frac{K_{A2-out}\cdot{}^{A2}K_{V1}}{K_{A2-total}} - K_{V1}\right). \quad [5]$$

**Kinetic Cooperative Circles.** The cooperative effects in the combined binding of **A1** and **V2** to **Zn1** were also investigated. **V2**, like **V1**, binds strongly to the inside of the cage of **Zn1** with a high association constant ($K_{V2} = 4.5 \times 10^6\ M^{-1}$) and comparable complexation geometry. A thermodynamic cooperative effect $Ce = 66$ was calculated from a $^1$H NMR titration of **A1** with the pseudorotaxane complex of **Zn1** with **V2** and an association constant $K_{V2A1} = 3.7 \times 10^{10}\ M^{-2}$ for the ternary complex formation. The difference between **V1** and **V2** is that in the latter case, because of the presence of the bulky cyclohexyl substituent, the kinetics of complex formation with **Zn1** via a slippage process can be monitored. Addition of **V2** to **Zn1** (0.8 $\mu$M) in various concentrations led to a decrease in porphyrin fluorescence emission in time, from which the slippage rate constant ($k_{on}$) and the equilibrium association constant ($K_{V2}$) of complex formation could be determined (Fig. 4*A*). To evaluate the cooperative effects on the kinetics of the slippage process, experiments were performed in the presence of various concentrations of **A1** (in excess compared with **Zn1**). All of the obtained kinetic curves could be fitted perfectly by 1:1 kinetic binding isotherms. In the presence of increasing concentrations of **A1**, which coordinates to the outside of **Zn1**, both the calculated values of $^{A1}k_{on\text{-}app}$ and $^{A1}K_{V2\text{-}app}$ increased. The thermodynamic data ($^{A1}K_{V2\text{-}app}$) was analyzed according to Eqs. **1** and **3**, revealing a cooperative effect of $Ce = 58$ and an association constant $K_{V2A1} = 3.3 \times 10^{10}\ M^{-2}$ (closely in line with the values of $Ce = 66$ and $K_{V2A1} = 3.7 \times 10^{10}\ M^{-2}$ obtained from the $^1$H NMR titrations). The slippage rate constants ($^{A1}k_{on\text{-}app}$) showed an increase ranging from a value of $6.4 \times 10^4\ M^{-1}s^{-1}$ in the absence of **A1** to a value of $4.2 \times 10^5\ M^{-1}s^{-1}$ in the presence of 6.4 mM of **A1**. The observed concentration dependency of the slippage rate constants clearly reveals that we are dealing again with apparent values. The data can be rationalized as follows. Because **A1** is present in excess compared with **Zn1**, the kinetics can be described by 1:1 kinetic binding

*This value is based on studies concerning the binding of **A1** and **A2** to a number of to reference zinc-porphyrins revealing that **A1** binds ≈1.6 times stronger to zinc porphyrins than **A2** in the used solvent mixture (see SI).

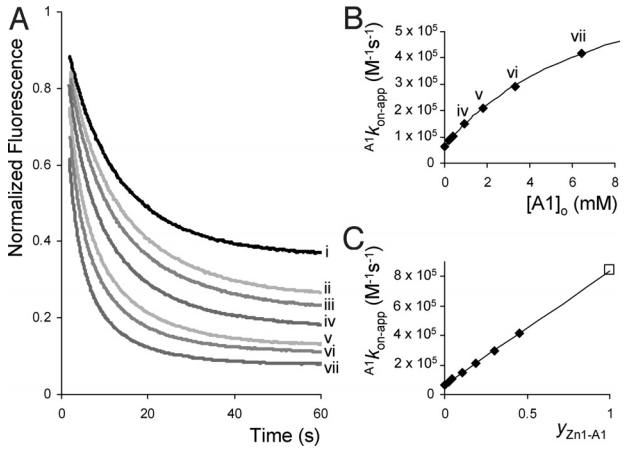


**Fig. 4.** Fluorescence slippage experiments between **V2** and **Zn1** in the presence of **A1**. (*A*) Fluorescence emission as a function of time upon the addition of 1 equivalent of **V2** to **Zn1** (0.8 $\mu$M) in the presence of increasing concentrations (from *i* to *vii*) of **A1**. (*B*) Calculated rate constants $^{A1}k_{on\text{-}app}$ plotted vs. the concentration of **A1** and the fit according to Eq. **7**. (*C*) Linear relationship between the value of $^{A1}k_{on\text{-}app}$ and the fractional saturation of **Zn1** with **A1** ($y_{Zn1\text{-}A1}$) according to Eq. **9**.

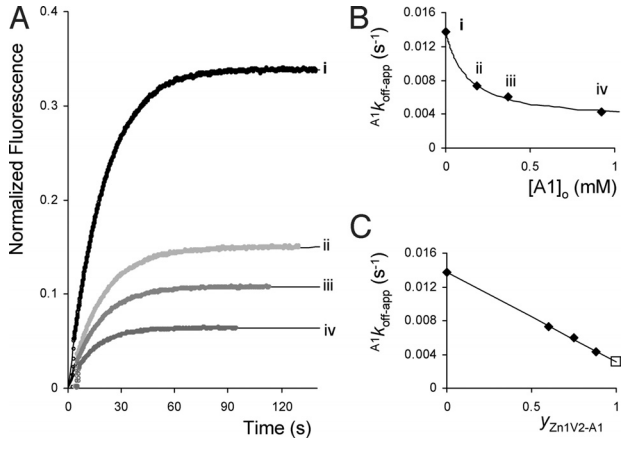


**Fig. 5.** Fluorescence deslippage experiments between **V2** and **Zn1** in the presence of **A1**. (*A*) Fluorescence emission as a function of time upon the dilution of a 1.5:1 mixture of **V2** and **Zn1** in the presence of increasing concentrations (from *i* to *iv*) of **A1**. (*B*) Calculated rate constants $^{A1}k_{off\text{-}app}$ plotted vs. the concentration of **A1** and the fit according to Eq. **8**. (*C*) Linear relationship between the value of $^{A1}k_{off\text{-}app}$ and the fractional saturation of the pseudorotaxane complex between **Zn1** and **V2** with **A1** ($y_{Zn1V2\text{-}A1}$) according to Eq. **10**.

isotherms (see Eq. **6**) in which $[\mathbf{Zn1_{tot}}] = [\mathbf{Zn1}] + [\mathbf{Zn1A1}]$, and $[\mathbf{Zn1V2_{tot}}] = [\mathbf{Zn1V2}] + [\mathbf{Zn1V2A1}]$ (see Fig. 1*C*).

$$v = -\frac{d[\mathrm{Znl_{tot}}]}{dt} = -\frac{d[\mathrm{V2}]}{dt} = \frac{d[\mathrm{ZnlV2_{tot}}]}{dt}$$

$$= {}^{A1}k_{\text{on-app}}[\mathrm{Znl_{tot}}][\mathrm{V2}] - {}^{A1}k_{\text{off-app}}[\mathrm{ZnlV2_{tot}}]. \qquad [6]$$

The observed experimental slippage rates $^{A1}k_{on\text{-}app}$ and $^{A1}k_{off\text{-}app}$ will display apparent values that depend on the concentration of pyridine **A1** according to Eqs. **7** and **8**.

$$^{A1}k_{\text{on-app}} = \frac{k_{\text{on}} + {}^{A1}k_{\text{on}} \cdot K_{A1} \cdot [\mathrm{A1}]}{1 + K_{A1} \cdot [\mathrm{A1}]} \qquad [7]$$

$$^{A1}k_{\text{off-app}} = \frac{k_{\text{off}} + {}^{A1}k_{\text{off}} \cdot {}^{V2}K_{A1} \cdot [\mathrm{A1}]}{1 + {}^{V2}K_{A1} \cdot [\mathrm{A1}]}. \qquad [8]$$

As required, the apparent association constant $^{A1}K_{V2}$ is the quotient of the slippage and deslippage rate constants ($^{A1}K_{V2\text{-}app} = {}^{A1}k_{on\text{-}app}/{}^{A1}k_{off\text{-}app}$) as illustrated by the fact that Eq. **1** is obtained when Eq. **7** is divided by Eq. **8**. Eq. **7** indeed nicely describes the experimentally determined slippage rate constants as can be seen in Fig. 4*B*, revealing a value of $^{A1}k_{on} = 8.4 \times 10^5\ M^{-1}s^{-1}$ and hence a cooperative kinetic effect of a factor of 13.2 ($ce_{(on)} = {}^{A1}k_{on}/k_{on}$). The slippage reaction is thus >13 times faster when **Zn1** is fully occupied on the outside by the coordinating ligand **A1**, whereas the binding constant $^{A1}K_{V2}$ is enhanced by a factor of ≈60. This thus indicates that the rate of pseudorotaxane dissociation (i.e., deslippage) in the presence of **A1** ($^{A1}k_{off}$) should be decreased by a factor of ≈4.

It is possible to directly measure the deslippage rate constants $k_{off}$ with the help of dilution experiments. Pseudorotaxane complexes were prepared at high (millimolar) concentrations after which the solutions were diluted to micromolar concentrations. As a result of this dilution, a new equilibrium situation is reached after a certain period, with less pseudorotaxane and more of the free components (See Fig. 5*A*). The increase in fluorescence emission as a result of dilution was recorded as a function of time, and the curves were analyzed. The presence of increasing concentrations of **A1** clearly resulted in lower deslippage rate constants ($^{A1}k_{off\text{-}app}$) and higher pseudorotaxane stabilities (hence higher values of $^{A1}K_{V2\text{-}app}$) as can be seen in Fig. 5*A*. From the calculated values of $^{A1}K_{V2\text{-}app}$ and $^{A1}k_{off\text{-}app}$, the magnitudes of the cooperative effects (*Ce* and $ce_{(off)}$) could be determined by applying Eqs. **1** and **8**. The resulting thermodynamic cooperative effect amounted to $Ce = 62$, in excellent agreement with the values of $Ce = 58$ and 66 mentioned above. $^{A1}k_{off}$ was calculated to be $3.1 \times 10^{-3}\ s^{-1}$, resulting in a cooperative kinetic effect for the deslippage process of $ce_{(off)} = {}^{A1}k_{off}/k_{off} = 0.23$ ($k_{off} = 1.4 \times 10^{-2}\ s^{-1}$), the expected reduction by a factor of 4. In line with theory, the combined kinetic cooperative effects for the slippage and deslippage reactions account for the full thermodynamic cooperative effect, i.e., $ce_{(on)}/ce_{(off)} = 58$ ($\Delta\Delta G^o = -10.0$ kJ/mole), which, within experimental error is identical to the cooperative effect of $Ce \approx 62$ ($\Delta\Delta G^o = -10.2$ kJ/mole) obtained from the thermodynamic studies. As observed above for the association constants, the value of $^{A1}k_{on\text{-}app}$ depends linearly on the fractional saturation of **Zn1** with **A1** ($y_{Zn1\text{-}A1}$), see Eq. **9** and Fig. 4*C*. The magnitude of $^{A1}k_{off\text{-}app}$ on the other hand, depends linearly on the fractional saturation of the pseudorotaxane complex formed by **Zn1** and **V2**, with **A1** ($y_{Zn1V2\text{-}A1}$), in line with Eq. **10** and illustrated in Fig. 5*C*.

$$^{A1}k_{\text{on-app}} = k_{\text{on}} \cdot \{1 + y_{\mathrm{Znl-A1}} \cdot (ce_{(\text{on})} - 1)\} \qquad [9]$$

$$^{A1}k_{\text{off-app}} = k_{\text{off}} \cdot \{1 + y_{\mathrm{ZnlV2-A1}} \cdot (ce_{(\text{off})} - 1)\}. \qquad [10]$$

Finally, the effects of blocking the cavity of **Zn1** with pyridine on the slippage rate constants were examined. To this end, slippage and deslippage experiments with **V2** and **Zn1** were performed in the presence of various concentrations of **A2** (Figs. 6 and 7). As observed for the combination, **A2**, **V1**, and **Zn1**, the apparent association constants $^{A2}K_{V2\text{-}app}$ decreased upon increasing the concentration of **A2** (see Fig. 7), revealing a linear dependency when these constants were plotted against the fractional saturation of **Zn1** with **A2** ($y_{Zn1\text{-}A2}$). A value of $K_{A2\text{-}out} \cdot {}^{A2}K_{V2} = K_{V2A2} = 1.6 \times 10^{10}\ M^{-2}$ was calculated by applying Eq. **4**, suggesting a cooperative effect for the combined binding of **V2** and **A2** to **Zn1** of $Ce \approx 45$ ($\Delta\Delta G^o = -9.4$ kJ/mole). The calculated slippage rate constants ($^{A2}k_{on\text{-}app}$) as expected revealed a decrease upon increasing the concentration of **A2** as a result of the blocking of the cavity of **Zn1**. The slippage rate constants could be fitted to Eq. **11** (Fig. 6*B*), which describes the evolution of $^{A2}k_{on\text{-}app}$ as a function of the concentration of **A2**.

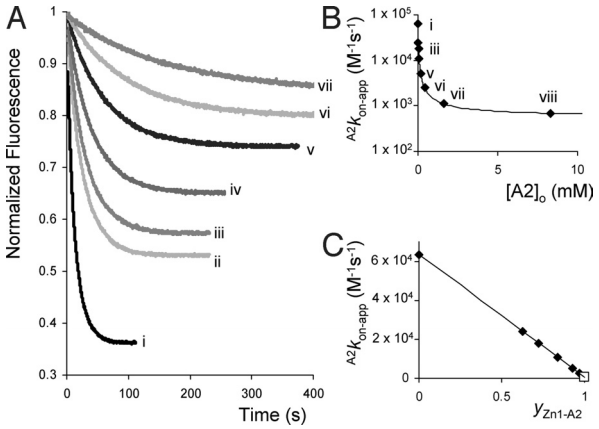


**Fig. 6.** Fluorescence slippage experiments between **V2** and **Zn1** in the presence of increasing concentrations of **A2**. (*A*) Fluorescence emission as a function of time upon the addition of 1 equivalent of **V2** to **Zn1** ($\mu$M) in the presence of increasing concentrations (from *i* to *vii*) of **A2**. (*B*) Calculated rate constants $^{A2}k_{on-app}$ plotted vs. the concentration of **A2** and the fit according to Eq. **11**. (*C*) Linear relationship between the value of $^{A2}k_{on-app}$ and the fractional saturation of **Zn1** with **A2** ($y_{Zn1-A2}$).

$$^{A2}k_{on-app} = \frac{k_{on} + [A2] \cdot K_{A2-out} \cdot {}^{A2}k_{on}}{1+[A2] \cdot K_{A2-total}}. \qquad [11]$$

The fact that upon full saturation of **Zn1** with **A2**, the slippage rate constant does not go to zero (see Figs. 6*B*) indicates that pyridine is indeed not solely coordinating to the inside of **Zn1** but also to the outside, in line with the binding scheme presented in Fig. 1 *B* and *D*. Assuming an association constant $K_{A2\text{-out}} = 80 \pm 15\ M^{-1}$, a value of $ce_{(on)} = 8.7$ ($\Delta\Delta G^{\neq}_{on} = -5.4$ kJ/mole) was obtained, which does not significantly deviate from the kinetic cooperative effect $ce_{(on)} = 13.2$ ($\Delta\Delta G^{\neq}_{on} = -6.4$ kJ/mole) observed for the combination **A1**, **V2**, and **Zn1**.

The 2 opposing effects of **A2**, namely, the competitive binding to the inside of the cavity of **Zn1** and the fact that this ligand increases the stability of the pseudorotaxane as a result of coordination of **A2** to the outside of **Zn1**, are clearly expressed in the deslippage curves (Fig. 7*A*). Increasing concentrations of **A2** drive the equilibrium further away from the nonfluorescent pseudorotaxane species in

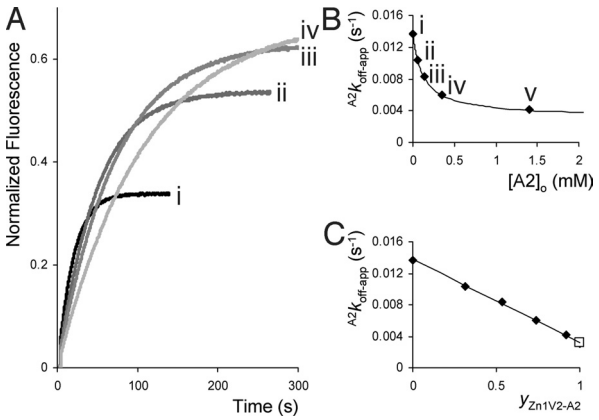


**Fig. 7.** Fluorescence deslippage experiments between **V2** and **Zn1** in the presence of increasing concentrations of **A2**. (*A*) Fluorescence emission as a function of time upon the dilution of a 1.5:1 mixture of **V2** and **Zn1** in the presence of increasing concentrations (from *i* to *iv*) of A2. (*B*) Calculated rate constants $^{A2}k_{off-app}$ plotted vs. concentration of **A2** and the fit according to Eq. **12**. (*C*) Linear relationship between the value of $^{A2}k_{off-app}$ and the fractional saturation of the pseudorotaxane complex between **Zn1** and **V2** with **A2** ($y_{Zn1V2-A2}$).

the direction of the fluorescent complex in which **A2** binds inside the cavity of **Zn1**. The rates of deslippage ($^{A2}k_{off-app}$) decrease concomitantly, indicating the increased stability of the pseudorotaxane as a result of the coordination of **A2** to the outside of the pseudorotaxane complex formed by **V2** and **Zn1**. The calculated dependency of the deslippage rate on the presence of **A2** ($^{A2}k_{off-app}$) revealed striking similarity with the dependency on **A1** ($^{A1}k_{off-app}$). Values of $^{A2}k_{off} = 3.2 \times 10^{-3}\ s^{-1}$, $ce_{(off)} = 0.23$, and $^{V2}K_{A2} = 8.1 \times 10^3\ M^{-1}$ were obtained by applying Eq. **12**, confirming that the role of **A2** is identical to that of **A1** when it coordinates to the outside of the pseudorotaxane complex formed by **Zn1** and **V2**.

$$^{A2}k_{off-app} = \frac{k_{off} + {}^{A2}k_{off} \cdot {}^{V2}K_{A2} \cdot [A2]}{1+{}^{V2}K_{A2} \cdot [A2]}. \qquad [12]$$

## Conclusion

The full thermodynamic and kinetic circles regarding both inhibition and activation of the cage of **Zn1** for the binding of viologens has been measured. Independent of the measured direction of the circles, identical values were observed, in accordance with theory. This therefore reveals the beautiful symmetry of the studied cooperative binding effects and moreover shows the accuracy of the used method. We have successfully demonstrated that the developed method can be used to uncover complete binding schemes from a series of (in principle only 3) simple 1:1 titration experiments. The method can be applied to a large number of different systems, both natural and artificial, and can be used to successfully uncover cooperative binding systems also when only 1 specific binding interaction can be monitored.

The combined binding of bulky pyridine **A1** and viologen derivatives to receptor **Zn1** is accompanied by a positive cooperative effect in the order of $\Delta\Delta G^{o} = -10$ kJ/mole. This thermodynamic effect is composed of a decrease in the free energy of activation of complex formation ($\Delta\Delta G^{\neq}_{on}$) of ≈6 kJ/mole and an increase in the free energy of activation of complex dissociation ($\Delta\Delta G^{\neq}_{off}$) of ≈4 kJ/mole. In other words, the rate of receptor–viologen complex formation is increased as a result of the coordination of **A1** to the outside, whereas the rate of complex dissociation is decreased. The situation is more complex in the case of pyridine **A2**. This ligand displays the same effect as **A1** when it is bound to the outside of **Zn1** but, when bound inside its cavity, it fully obstructs the binding of the viologen derivatives. This inhibition is expressed in the measured equilibrium association constants and in the rates of pseudorotaxane complex formation. The presented results underline the apparent character of the experimentally determined rate and association constants. The obtained cooperative effects in most cases do not reveal their actual values. Only when a receptor is fully occupied by a guest (that is, when the fractional saturation of the receptor with this guest equals 1), the experimentally determined value equals the actual cooperative binding effect. In all other cases, the observed value of the effect depends linearly on the fractional saturation of the receptor. As a result of this, many of the values of heterotropic cooperative binding effects reported in the literature may in fact deviate significantly from the actual values.

The inhibition experiments performed with pyridine further highlight the effect competitive binding has on observed association and rate constants. Competing interactions lead to apparent association constants ($K_{G\text{-app}}$) that relate to their actual values ($K_G$) according to Eq. **13**, in which X is the concentration of the competing species, and $K_X$ is the association constant of the complex between this species with the receptor.

$$K_{G-app} = \frac{K_G}{1+K_X \cdot [X]}. \qquad [13]$$

It is clear that in the case of high concentrations of X, only low values of $K_X$ are needed to significantly change the experimental outcome. Especially in studies involving coordination of ligands to

metal centers, weakly coordinating electron donating solvent molecules can dramatically influence the experimentally observed association constants. Consider, for instance, water as a solvent with a molarity of 55. If water binds to the metal center with an association constant of only 0.5 $M^{-1}$ [a value that is generally considered to be random and therefore of little significance (31)], this will cause an apparent association constant for any titrated ligand that is 28.5 times lower than its actual magnitude (a difference of 8.3 kJ/mole). Also when high salt concentrations are present, the experimentally observed values may differ significantly from the actual magnitudes; hence, the free binding energies are always related to the medium in which the measurements were carried out.

In summary, the studied system is a clear example of how binding events and reaction rates can be tuned in a supramolecular fashion and hence provides a simple mimic of supramolecular information transfer in nature. It furthermore shows how cooperative binding effects are experimentally expressed in the kinetics and thermodynamics of complex formation. The described method can be used to accurately study heterotropic cooperative binding effects in any natural or artificial system and can be seen as a simple framework to derive the actual magnitudes of these effects from the experimentally obtained values.

## Materials and Methods

See supporting information (SI) *Appendix*, Scheme S1, Figs. S1–S6, and Table S1 for full experimental details on the synthesis and characterization of the compounds used in this study and on the measurement methods.

**Association Constants.** Association equilibrium constants were determined by standard procedures (24) in which it was made sure that in the course of a titration experiment with a guest, the concentrations of the receptor and the second guest present in solution were kept constant.

**Slippage Kinetics.** Slippage kinetics were performed by using the time drive application of the spectrometer software. The sample was excited at 426 nm, and the porphyrin emission at 607 nm was recorded in time. Typically, to a weighed solution of 0.8 $\mu$M **Zn1**, a known amount of **V2** was added and the solution was mixed. After mixing (1.5 s), the measurement was started. The data were analyzed according to standard 1:1 kinetic isotherms involving complex formation between A and B, resulting in formation of C (Eqs. **14**-**17**) (32). From the fit, both the rate constant $k_{on}$ and equilibrium association constant $K_{assoc}$ were obtained.

All of the experiments were performed at least in triplicate and at different concentrations of **V2** to lower the experimental error.

$$\mathrm{A} + \mathrm{B} \underset{k_{off}}{\overset{k_{on}}{\rightleftharpoons}} \mathrm{C} \qquad [14]$$

$$[\mathrm{C}] = p\frac{\left(1 - \frac{q}{p}\frac{p - [C]_o}{q - [C]_o}e^{k_{on}(p-q)t}\right)}{\left(1 - \frac{p - [C]_o}{q - [C]_o}e^{k_{on}(p-q)t}\right)} \qquad [15]$$

$$p = [\mathrm{C}]_{eq} = \frac{([\mathrm{A}]_o + [\mathrm{B}]_o + \frac{1}{K_{assoc}}) - \sqrt{([\mathrm{A}]_o + [\mathrm{B}]_o + \frac{1}{K_{assoc}})^2 - 4\cdot[\mathrm{A}]_o\cdot[\mathrm{B}]_o}}{2} \qquad [16]$$

$$q = \frac{[\mathrm{A}]_o[\mathrm{B}]_o}{[\mathrm{C}]_{eq}} \qquad [17]$$

$$K_{assoc} = \frac{[\mathrm{C}]_{eq}}{([\mathrm{A}]_o - [\mathrm{C}]_{eq})\cdot([\mathrm{B}]_o - [\mathrm{C}]_{eq})} = \frac{k_{on}}{k_{off}}. \qquad [18]$$

**Deslippage Kinetics.** Solutions of **Zn1** and **V2** (approximately millimolar) in 1:1 (vol/vol) mixtures of $CDCl_3$ and $CD_3CN$ were prepared and a $^1$H-NMR spectrum was recorded establish the exact stochiometries. These solutions were added to a 1:1 (vol/vol) mixture of chloroform and acetonitrile, thereby diluting the pseudorotaxane concentration (**Zn1V2** = $\mu$M) to preset values. The sample was excited at 426 nm, and emission at 607 was recorded as a function of time by using the time drive application of the spectrometer software. After the experiment, a UV-vis spectrum was recorded to confirm the exact experimental concentrations of the species. The obtained deslippage curves were analyzed with the help of Eqs. **14**-**17**, assuming the relation $K_{assoc} = k_{on}/k_{off}$. The fits provided the values of both $k_{off}$ and $K_{assoc}$. All experiments were performed in triplicate to lower the experimental error.

**ACKNOWLEDGMENTS.** This work was supported by a National Research School Combination Catalysis Controlled by Chemical Design grant, Nederlandse Organisatie voor Wetenschappelijk Onderzoek, Vidi and Vici grants (J.A.A.W.E. and A.E.R.), a Koninklijke Nederlandse Akademie van Wetenschappen grant (R.J.M.N.), and a Nanoned grant (A.E.R. and R.J.M.N.).

1. Changeux J-P, Edelstein SJ (2005) Allosteric mechanisms of signal transduction. *Science* 308:1424–1428.
2. Klug A (1983) From macromolecules to biological assemblies (Nobel lecture). *Angew Chem Int Ed Engl* 22:565–582.
3. Ackers GK, Doyle ML, Myers D, Daugherty MA (1992) Molecular code for cooperativity in hemoglobin. *Science* 255:54–63.
4. Williams DH, Stephens E, O'Brien DP, Zhou M (2004) Understanding noncovalent interactions: Ligand binding energy and catalytic efficiency from ligand-induced reductions in motion within receptors and enzymes. *Angew Chem Int Ed* 43:6596–6616.
5. Traylor TG, Mitchell MJ, Ciconene JP, Nelson S (1982) Cooperativity in chemical model systems: Ligand-induced subunit dimerization. *J Am Chem Soc* 104:4986–4989.
6. Tabushi I, Sasaki T (1983) Cooperative dioxygen binding by cobalt(II) gable porphyrin in homogeneous solution. *J Am Chem Soc* 105:2901–2902.
7. Rebek J, et al. (1985) Allosteric effects in organic chemistry: Binding cooperativity in a model for subunit interactions. *J Am Chem Soc* 107:7481–7487.
8. Ayabe M, Ikeda A, Kubo Y, Takeuchi M, Shinkai S (2002) A dendritic porphyrin receptor for C60 which features a profound positive allosteric effect. *Angew Chem Int Ed* 41:2790–2792.
9. Takeuchi M, Imada T, Shinkai S (1996) Highly selective and sensitive ''sugar tweezer'' designed from a boronic-acid-appended $\mu$-oxo-bis[porphinatoiron(III)]. *J Am Chem Soc* 118:10658–10659.
10. Thordarson P, et al. (2003) Highly negative homotropic allosteric binding of viologens in a double-cavity porphyrin. *J Am Chem Soc* 125:1186–1187.
11. Sato H, Tashiro K, Shinmori H, Osuka A, Aida T (2005) Cyclic dimer of a fused porphyrin zinc complex as a novel host with two $\pi$-electronically coupled binding sites. *Chem Commun* 18:2324–2326.
12. Rebek J, Wattley RV (1980) Allosteric effects. Remote control of ion transport selectivity. *J Am Chem Soc* 102:4853–4854.
13. Sijbesma RP, Nolte RJM (1991) A molecular clip with allosteric binding properties. *J Am Chem Soc* 113:6695–6696.
14. Kobuke Y, Satoh Y (1992) Positive cooperativity in cation binding by novel polyether-bis(.beta.-diketone) hosts. *J Am Chem Soc* 114:789–790.
15. Schneider H-J, Ruf D (1990) A synthetic allosteric system with high cooperativity between polar and hydrophobia binding sites. *Angew Chem Int Ed* 29:1159–1160.
16. Baldes R, Schneider H-J (1995) Complexes from polyazacyclophanes, fluorescence indicators, and metal cations—An example of allosterism through ring contraction. *Angew Chem Int Ed* 34:321–323.
17. Thordarson P, et al. (2004) Allosterically driven multicomponent assembly. *Angew Chem Int Ed* 43:4755–4759.
18. Sato H, et al. (2005) Positive heterotropic cooperativity for selective guest binding via electronic communications through a fused zinc porphyrin array. *J Am Chem Soc* 127:13086–13087.
19. Heo J, Mirkin CA (2006) Pseudo-allosteric recognition of mandelic acid with an enantioselective coordination complex. *Angew Chem Int Ed* 45:941–944.
20. Darbost U, et al. (2007) Allosteric tuning of the intra-cavity binding properties of a calix[6]arene through external binding to a ZnII center coordinated to amino side chains. *Chem Eur J* 13:2078–2088.
21. Deng D, James TD, Shinkai S (1994) Allosteric interaction of metal ions with saccharides in a crowned diboronic acid. *J Am Chem Soc* 116:4567–4572.
22. Al-Sayah MH, Branda NR (2000) Metal ions as allosteric inhibitors in hydrogenbonding receptors. *Angew Chem Int Ed* 39:945–947.
23. Tobey SL, Anslyn EV (2003) Studies into the thermodynamic origin of negative cooperativity in ion-pairing molecular recognition. *J Am Chem Soc* 125:10963–10970.
24. Elemans JAAW, et al. (1999) Porphyrin clips derived from diphenylglycoluril. Synthesis, conformational analysis, and binding properties. *J Org Chem* 64:7009–7016.
25. Elemans JAAW, Bijsterveld EJA, Rowan AE, Nolte RJM (2007) Manganese porphyrin hosts as epoxidation catalysts–Activity and stability control by .axial ligand effects. *Eur J Org Chem* 751–757.
26. Harrison IT (1972) The effect of ring size on threading reactions of macrocycles. *J Chem Soc Chem Commun* 231–232.
27. Händel M, Plevots M, Gestermann S, Vögtle F (1997) Synthesis of rotaxanes by brief melting of wheel and axle components. *Angew Chem Int Ed Engl* 36:1199–1201.
28. Ashton PR, Bělohradsky M, Philp D, Spencer N, Stoddart JF (1993) The selfassembly of [2]- and [3]rotaxanes by slippage. *J Chem Soc Chem Commun* 16:1274–1277.
29. Amabilino DB, Ashton PR, Bělohradsky M, Raymo FM, Stoddart JF (1995) The self-assembly of branched [n]rotaxanes - the first step towards dendritic rotaxanes. *J Chem Soc Chem Commun* 7:751–753.
30. Ricard J, Cornish-Bowden A (1987) Co-operative and allosteric enzymes: 20 years on. *Eur J Biochem* 166:255–272.
31. Conners KA (1987) in *Binding Constants* (Wiley, New York), pp 89–93.
32. Koppelman SJ, et al. (1996) Requirements of von Willebrand factor to protect factor VIII from inactivation by activated protein C. *Blood* 87:2292–2300.